

Hadronic vacuum polarization contribution to the muon $g-2$ in holographic QCD

Josef Leutgeb^{⊗,1,*}, Anton Rebhan^{⊗,1,†} and Michael Stadlbauer^{⊗,1,2,3,‡}

¹*Institut für Theoretische Physik, Technische Universität Wien,
Wiedner Hauptstrasse 8-10, A-1040 Vienna, Austria*

²*Technische Universität München, Physik-Department,
James-Franck-Strasse 1, 85748 Garching, Germany*

³*Max Planck Institute for Physics, Föhringer Ring 6, 80805 München, Germany*



(Received 11 April 2022; accepted 23 April 2022; published 25 May 2022)

We evaluate the leading-order hadronic vacuum polarization contribution to the anomalous magnetic moment of the muon with two light flavors in minimal hard-wall and soft-wall holographic QCD models, as well as in simple generalizations thereof, and compare it to the rather precise results available from dispersive and lattice approaches. While holographic QCD cannot be expected to shed light on the existing small discrepancies between the latter, this comparison in turn provides useful information on the holographic models, which have been used to evaluate hadronic light-by-light contributions where errors in data-driven and lattice approaches are more sizable. In particular, in the hard-wall model that has recently been used to implement the Melnikov-Vainshtein short-distance constraint on hadronic light-by-light contributions, a matching of the hadronic vacuum polarization to the data-driven approach points to the same correction of parameters that has been proposed recently in order to account for next-to-leading-order effects.

DOI: [10.1103/PhysRevD.105.094032](https://doi.org/10.1103/PhysRevD.105.094032)

I. INTRODUCTION

Currently there is a 4.2σ discrepancy between the Standard Model prediction for the anomalous magnetic moment of the muon $a_\mu = (g-2)_\mu/2$ as assembled in the white paper (WP) [1] and the new experimental result, obtained by combining the Brookhaven National Laboratory and Fermilab E989 values, involving an experimental error of 41×10^{-11} , which is expected to be reduced further by additional data taking and future experiments. The uncertainty in the Standard Model prediction has a similar magnitude; it is almost entirely due to hadronic contributions from hadronic vacuum polarization (HVP) and hadronic light-by-light scattering (HLbL), which according to [1] amount to

$$a_\mu^{\text{HVP,WP}} = (6845 \pm 40) \times 10^{-11}, \quad (1.1)$$

$$a_\mu^{\text{HLbL,WP}} = (92 \pm 19) \times 10^{-11}. \quad (1.2)$$

The data-driven computation of HVP thus claims an accuracy of 0.6%, whereas the much smaller HLbL contribution has about 20% uncertainty. To match the experimental progress, improvements in the theoretical predictions for both contributions are called for.

However, the data-driven HVP result was recently questioned using a direct lattice QCD calculation [2] by the BMW Collaboration, which claims a similar error of 0.8%,

$$a_\mu^{\text{HVP,BMW}} = (7075 \pm 55) \times 10^{-11}, \quad (1.3)$$

but deviates from Eq. (1.1) by about 3% or 2.1σ . Replacing Eq. (1.1) with Eq. (1.3) would reduce the discrepancy between experiment and theory in the case of a_μ to about 1.5σ , while it may give rise to tensions with electroweak precision fits of the hadronic contribution to the running of the electromagnetic coupling [3–5].

Once this critical issue has been resolved, it will also be crucial to reduce the theoretical uncertainty in the HLbL contribution. In the latter, an important question has been the implementation of certain short-distance constraints in hadronic models [6–8], where recently holographic QCD has helped to shed light on the role of axial-vector mesons [9–12]. Holographic QCD also makes interesting quantitative predictions given the large spread of results in

*josef.leutgeb@tuwien.ac.at
†anton.rebhan@tuwien.ac.at
‡michael.stadlbauer@tum.de

Published by the American Physical Society under the terms of the [Creative Commons Attribution 4.0 International license](https://creativecommons.org/licenses/by/4.0/). Further distribution of this work must maintain attribution to the author(s) and the published article's title, journal citation, and DOI. Funded by SCOAP³.

other hadronic models, which have led to a 100% uncertainty for the estimated contribution of axial-vector mesons in the WP. Being an approach which is based on the large color number N_c limit, it cannot be expected to help with the percent-level discrepancies in the highly constrained HVP contribution. However, given that it typically achieves an accuracy of 10%–20%, it can provide potentially useful information in the case of HLbL. Investigating the performance in the case of HVP allows us to test the holographic QCD models with regard to their ability to describe photon-hadron interactions quantitatively.

In this paper we evaluate the leading-order (LO) HVP contribution of the minimal bottom-up holographic QCD models that have been employed in the study of the HLbL contribution, as well as simple generalizations thereof, and compare it to relevant results obtained within the data-driven approach, in particular those for the contributions of the lightest quark flavors, thereby revisiting and extending the study of Hong *et al.* [13].

As shown in [14,15], the leading-order HVP contributions to the muon $g - 2$ is related to the hadronic vacuum polarization function through

$$a_\mu^{\text{LO-HVP}} = 4\pi^2 \left(\frac{\alpha}{\pi}\right)^2 \int_0^\infty dQ^2 f(Q^2) \Pi_{\text{em}}^{\text{had}}(Q^2), \quad (1.4)$$

where $Q^2 = -q^2$ is the Euclidean momentum squared and

$$f(Q^2) = \frac{m_\mu^2 Q^2 Z^3 (1 - Q^2 Z)}{1 + m_\mu^2 Q^2 Z^2},$$

$$Z = -\frac{Q^2 - \sqrt{Q^4 + 4m_\mu^2 Q^2}}{2m_\mu^2 Q^2}. \quad (1.5)$$

The hadronic vacuum polarization function needs to be renormalized such that $\Pi_{\text{em}}^{\text{had}}(0) = 0$. It is given by the vector-current correlator, which is defined by

$$i \int d^4x e^{iqx} \langle 0 | T \{ J_V^{a\mu}(x) J_V^{b\nu}(0) \} | 0 \rangle$$

$$= \delta^{ab} (q^2 \eta^{\mu\nu} - q^\mu q^\nu) \Pi_V(-q^2) \quad (1.6)$$

in the flavor-symmetric case, via

$$\Pi_{\text{em}}^{\text{had}}(-q^2) = 2\text{Tr} Q_{\text{em}}^2 \Pi_V(-q^2), \quad (1.7)$$

where $Q_{\text{em}} = \text{diag}(\frac{2}{3}, -\frac{1}{3}, \dots)$ is the quark charge matrix.

As we shall show, the holographic results can deviate by up to 50% from the data-driven result, even after accounting for the fact that the holographic QCD results, being essentially a large- N_c approximation, can account for only a subset of multihadron intermediate states. However, the simplest hard-wall (HW) model that can simultaneously fit the rho meson mass and the pion decay constant, as well as

the leading-order short-distance behavior of the vector correlator, is performing quite reasonably. Interestingly, the amount of correction expected from next-to-leading-order effects in the large-momentum domain, where perturbative corrections to the asymptotic behavior proportional to α_s/π should play a role, turn out to be consistent with the corrections proposed recently by two of us in the case of the HLbL contribution [11].

In the next section, we shall review the minimal holographic QCD models included in our study to the extent necessary for evaluating the LO-HVP contribution to a_μ in Sec. III. Section IV summarizes our conclusions.

II. MINIMAL HOLOGRAPHIC QCD MODELS

In this work we shall limit ourselves to holographic QCD models with a minimal set of adjustable parameters with anti-de Sitter background geometry and simple generalizations thereof.

A. Hard-wall models

In HW AdS/QCD models, a five-dimensional anti-de Sitter (AdS) background geometry is chosen. In terms of a holographic radial coordinate z where the conformal boundary is at $z = 0$, the line element is given by (using a mostly minus metric convention)

$$ds^2 = g_{MN} dx^M dx^N = \frac{1}{z^2} (\eta_{\mu\nu} dx^\mu dx^\nu - dz^2), \quad 0 < z \leq z_0. \quad (2.1)$$

Conformal invariance is broken by a hard cutoff at $z = z_0$, where suitable boundary conditions for bulk fields dual to the quantum operators of the four-dimensional (large- N_c) gauge theory are imposed.

The fields dual to left and right quark bilinears $\bar{\psi} \gamma^\mu T^a P_{L,R} \psi$ are five-dimensional $U(N_f)_{L,R}$ gauge fields $A^{(L,R)}$, where chiral symmetry breaking can be implemented through spontaneous symmetry breaking by a bifundamental scalar X [16,17] or through different boundary conditions [18] on vector and axial-vector fields, $V = \frac{1}{2}[A^{(L)} + A^{(R)}]$ and $A = \frac{1}{2}[A^{(L)} - A^{(R)}]$, or both [19].

The five-dimensional action of models with a bifundamental scalar X introduced first by Erlich *et al.* [16] (termed HW1 in the following) reads

$$S = \int d^5x \sqrt{g} \text{Tr} \left\{ |DX|^2 + 3|X|^2 - \frac{1}{4g_5^2} (F_L^2 + F_R^2) \right\}, \quad (2.2)$$

whereas the model of Hirn and Sanz [18] (termed HW2) has only the Yang-Mills part.

In both cases, the field equations for transverse vector fields $\partial_\mu V^\mu = 0$ are given by

$$\partial_z \left(\frac{1}{z} \partial_z V_\mu^a(q, z) \right) + \frac{q^2}{z} V_\mu^a(q, z) = 0, \quad (2.3)$$

where we have Fourier transformed with respect to the spacetime coordinates of the boundary theory. Splitting the vector field further as $V_\mu^a(q, z) = V(q, z)v_\mu^a$, one can interpret the on-shell action, given by the boundary term

$$S = -\frac{1}{2g_5^2} \int d^4x \left(\frac{1}{z} V_\mu^a \partial_z V^{\mu a} \right) \Big|_{z=\epsilon}, \quad (2.4)$$

as the generating functional for QCD flavor currents. In both the HW1 and HW2 models, boundary conditions on V are such that there is no contribution from $z = z_0$, while the conformal boundary at $z = 0$ needs regularization by a finite cutoff $z = \epsilon$ when $V(q, \epsilon) = 1$ is imposed.

Thus we find that

$$\Pi_V(-q^2) = -\frac{1}{g_5^2 q^2} \frac{\partial_z V(q, z)}{z} \Big|_{z=\epsilon}. \quad (2.5)$$

The equations of motion (2.3) can be solved in terms of Bessel functions. Using the boundary conditions $V(q, \epsilon) = 1$ and $\partial_z V(q, z)|_{z=z_0} = 0$ yields

$$V(q, z) = \frac{z J_1(qz) Y_0(qz_0) - z Y_1(qz) J_0(qz_0)}{\epsilon J_1(q\epsilon) Y_0(qz_0) - \epsilon Y_1(q\epsilon) J_0(qz_0)} \Big|_{\epsilon \rightarrow 0}. \quad (2.6)$$

Plugging this result into Eq. (2.5) yields

$$\Pi_V(-q^2) = -\frac{1}{g_5^2} \frac{1}{q\epsilon} \frac{J_0(qz_0) Y_0(q\epsilon) - Y_0(qz_0) J_0(q\epsilon)}{J_0(qz_0) Y_1(q\epsilon) - Y_0(qz_0) J_1(q\epsilon)}, \quad (2.7)$$

and expanding this at $\epsilon \rightarrow 0$ gives

$$\Pi_V(-q^2) = \frac{1}{g_5^2} \left[-\frac{\pi Y_0(qz_0)}{2 J_0(qz_0)} + \gamma - \ln 2 + \ln q\epsilon + \mathcal{O}(\epsilon^2) \right], \quad (2.8)$$

where γ is the Euler-Mascheroni constant. This expression is divergent for $\epsilon \rightarrow 0$ and has to be renormalized. Adding a counterterm

$$S_{\text{c.t.}}(\mu) = \int d^4x \left(\frac{1}{2g_5^2} \ln \epsilon \mu \right) \text{Tr}[F_{\mu\nu}(x, \epsilon)]^2 \quad (2.9)$$

to the action gives rise to an additional term

$$\Pi_V^{\text{c.t.}} = -\frac{1}{g_5^2} \ln(\mu\epsilon), \quad (2.10)$$

which cancels the divergent part of Eq. (2.8). The resulting renormalized vacuum polarization is

$$\begin{aligned} \Pi_V^{\text{ren}}(-q^2) &= \lim_{\epsilon \rightarrow 0} [\Pi_V(-q^2) + \Pi_V^{\text{c.t.}}(-q^2)] \\ &= \frac{1}{g_5^2} \left[-\frac{\pi Y_0(qz_0)}{2 J_0(qz_0)} + \gamma + \ln \frac{q}{2\mu} \right], \end{aligned} \quad (2.11)$$

where μ can be chosen such that $\Pi_V^{\text{ren}}(0) = 0$ holds, as required for α in Eq. (1.4) to be identified with the standard fine structure constant in the Thomson limit. For Euclidean momenta this yields

$$\Pi_V^{\text{ren}}(Q^2) = \frac{1}{g_5^2} \left[\frac{K_0(Qz_0)}{I_0(Qz_0)} + \ln \frac{Qz_0}{2} + \gamma \right]. \quad (2.12)$$

As can be seen in Eq. (2.11), in the timelike domain the vacuum polarization function has an infinite series of poles at $q^2 = m_n^2$ with m_n determined by $J_0(m_n z_0) = 0$, corresponding to an infinite tower of (stable) vector mesons (as expected in a large- N_c limit). The latter are described by normalizable solutions of

$$\partial_z \left(\frac{1}{z} \partial_z \psi_n \right) + \frac{m_n^2}{z} \psi_n = 0, \quad (2.13)$$

with boundary conditions $\psi_n'(z_0) = 0$, $\psi_n(0) = 0$, and are explicitly given by

$$\psi_n(z) = \frac{\sqrt{2} z J_1(m_n z)}{z_0 J_1(m_n z_0)}. \quad (2.14)$$

The unrenormalized vector-current correlator can then be represented as

$$\Pi_V(q^2) = \sum_{n=1}^{\infty} \frac{F_n^2}{(q^2 - m_n^2) m_n^2}, \quad (2.15)$$

with decay constants F_n , defined as $\langle 0 | J_V^{a\mu}(0) | V_n^b \rangle = F_n \delta^{ab} \epsilon^\mu$, given by

$$F_n = \lim_{\epsilon \rightarrow 0} \frac{1}{g_5} \psi_n'(\epsilon) / \epsilon = \frac{1}{g_5 z_0} \frac{\sqrt{2} m_n}{J_1(m_n z_0)}. \quad (2.16)$$

1. Parameters of the HW1 model

In the chiral limit, the HW1 model has only three free parameters, g_5 , z_0 , and the chiral condensate described by $X(z_0)$. In the application to HLbL contributions [9], those were matched to the pion decay constant f_π , the ρ meson mass, and g_5 was set such that the short-distance constraint on Π_V from QCD [20,21],

$$\begin{aligned} \Pi_V(Q^2) &= \frac{N_c}{24\pi^2} \left(1 + \frac{\alpha_s}{\pi} \right) \ln \left(\frac{Q^2}{\mu^2} \right) - \frac{\alpha_s}{24\pi} \frac{N_c}{3} \frac{\langle G^2 \rangle}{Q^4} \\ &+ \frac{14N_c \pi \alpha_s \langle q\bar{q} \rangle^2}{27 Q^6}, \end{aligned} \quad (2.17)$$

is satisfied to leading order.¹ This determines

$$\frac{1}{g_5^2} = \frac{N_c}{12\pi^2}, \quad (2.18)$$

which holds true in other bottom-up models with a bulk geometry that is at least asymptotically AdS.

The HW cutoff z_0 directly determines the mass of the lightest vector meson, which we choose as $m_\rho = 775$ MeV, corresponding to

$$z_0 = 3.103 \text{ GeV}^{-1}. \quad (2.19)$$

This remains unchanged when finite quark masses are introduced in the HW1 model; the latter modify, however, axial-vector meson masses and vector meson masses with open flavor quantum numbers [23].

2. Parameters in the HW2 model

In the inherently chiral HW2 model of Hirn and Sanz [18], chiral symmetry breaking is implemented without a symmetry breaking bifundamental scalar X through different boundary conditions for vector and axial-vector fields.

When g_5 and z_0 are chosen as above, the pion decay constant can no longer be fitted to phenomenological values. In the application to HLbL contributions for the muon anomalous magnetic moment [9,10,24,25], which are dominated by the coupling of pions to two photons, f_π is fixed first, leaving the choice of matching either the infrared parameter m_ρ through z_0 or the ultraviolet behavior through g_5 . In [9,25], the former option, with physical values for f_π and m_ρ , is referred to as the HW2 model. This matches the short-distance constraints on transition form factors and also the Melnikov-Vainshtein short-distant constraint [6] only at a level of 61%. Conversely, the leading term in Eq. (2.17) is too large at the level of 164%. Matching these constraints at the expense of a much too heavy rho meson (987 MeV) was called HW2(UV fit).²

The symmetry breaking boundary conditions can in fact also be used in conjunction with the symmetry breaking scalar X . This possibility was proposed in [19] and also explored in [11] for HLbL contributions to a_μ , where it was referred to as HW3. In the vector sector, however, this

coincides with the HW1 model, so our HVP results for the latter also pertain to the HW3 case.

Summarizing the values of the parameters for the three different fits we have, for $N_c = 3$,

$$\begin{aligned} \text{HW1: } g_5 &= 2\pi, & z_0 &= 3.103 \text{ GeV}^{-1}, \\ \text{HW2: } g_5 &= 4.932, & z_0 &= 3.103 \text{ GeV}^{-1}, \\ \text{HW2 (UV fit): } g_5 &= 2\pi, & z_0 &= 2.4359 \text{ GeV}^{-1}. \end{aligned} \quad (2.20)$$

B. Soft-wall (SW) model

A shortcoming of the HW models is that the masses of highly excited vector mesons do not rise as $m_n^2 \sim \sigma n$ as expected from linear confinement with the string constant σ , but instead like $m_n^2 \sim n^2$.

The so-called soft-wall model introduced in [26] (a precursor of which appeared in [27]) achieves a strictly linear dependence of m_n^2 on n by introducing a dilaton $\Phi(z) = \kappa^2 z^2$ as an additional background field in the five-dimensional Lagrangian [26,28]

$$S = \int d^5x e^{-\Phi(z)} \sqrt{g} \text{Tr} \left\{ |DX|^2 + 3|X|^2 - \frac{1}{2g_5^2} (F_L^2 + F_R^2) \right\} \quad (2.21)$$

while keeping the AdS metric (2.1). The z coordinate is, however, now unbounded from above, $z \in [0, \infty)$.

Solving the correspondingly modified field equation

$$\partial_z \left(\frac{e^{-\Phi}}{z} \partial_z V_\mu^a \right) + \frac{q^2 e^{-\Phi}}{z} V_\mu^a = 0 \quad (2.22)$$

with the boundary conditions $V(q, \epsilon) = 1$ in the limit $\epsilon \rightarrow 0$ and $\lim_{z \rightarrow \infty} V(q, z) = 0$ gives [29]

$$V(q, z) = \Gamma \left(1 - \frac{q^2}{4\kappa^2} \right) U \left(\frac{-q^2}{4\kappa^2}, 0, (\kappa z)^2 \right), \quad (2.23)$$

with the confluent hypergeometric function of the second kind U (also known as the Tricomi function). Plugging this into

$$\Pi_V(-q^2) = - \frac{e^{-\Phi} \partial_z V(q, z)}{g_5^2 q^2 z} \Big|_{z=\epsilon}, \quad (2.24)$$

switching to the Euclidean momentum $Q^2 = -q^2$, and expanding in a series for small ϵ gives

$$\Pi_V(Q^2) = \frac{1}{2g_5^2} \left[\psi \left(\frac{Q^2}{4\kappa^2} + 1 \right) + \ln(\kappa^2 \epsilon^2) + 2\gamma \right] + \mathcal{O}(\epsilon), \quad (2.25)$$

¹See [22] for a modification of the HW1 model which aims to incorporate the effects from the gluon condensate $\langle G^2 \rangle$.

²These two choices correspond essentially to the parameters in “set 1” and “set 2” of [10], where only the Hirn-Sanz model was considered.

where $\psi(z) = d \ln \Gamma(z)/dz$. Renormalizing as above and using $\psi(0) = -\gamma$, we find that

$$\Pi^{\text{ren}}(Q^2) = \frac{1}{2g_5^2} \left[\psi \left(\frac{Q^2}{4\kappa^2} + 1 \right) + \gamma \right], \quad (2.26)$$

with g_5 fixed as in the HW1 model.

From the poles of the digamma function ψ one can see that the spectrum of vector mesons is now given by

$$m_n^2 = 4\kappa^2 n, \quad n = 1, 2, 3, \dots \quad (2.27)$$

Alternatively, the hadronic vacuum polarization can be calculated as above from the normalizable solutions given by [26,29]

$$\psi_n(z) = \sqrt{\frac{2}{n}} \kappa^2 z^2 L_{n-1}^1(\kappa^2 z^2), \quad (2.28)$$

where the L_n^1 are the generalized Laguerre polynomials of order 1, leading to the decay constants

$$F_n = \frac{1}{g_5} \psi_n''(0) = \frac{1}{g_5} \kappa^2 \sqrt{8n}. \quad (2.29)$$

C. Interpolating models

The phenomenological study of pion form factors for HW and SW models in [28] led to the conclusion that the HW1 model generally performed better than the SW model. In [28,30], a simple interpolating model was proposed that combines features of HW and SW models, whereas in [31–33] a more sophisticated version including a dynamical tachyon for chiral symmetry breaking was developed, which achieves a similar behavior.

1. Semihard-wall (SHW) model

In the model proposed by Kwee and Lebed in [28,30], a semihard wall was set up by replacing the dilaton background of the SW model $e^{-\Phi} = e^{-\kappa^2 z^2}$ with a background given by

$$e^{-\Phi(z)} = \frac{e^{\lambda^2 z_0^2} - 1}{e^{\lambda^2 z_0^2} + e^{\lambda^2 z^2} - 2}. \quad (2.30)$$

The HW model is recovered by $\lambda z_0 \rightarrow \infty$ at a fixed z_0 , whereas at large z the dilaton behaves as $\Phi(z) \sim \lambda^2 z^2$.

In [30] two sets of parameters were considered, involving $\lambda z_0 = 2.1$ and 1, where the first choice was found to display a good agreement with the pion form factor $F_\pi(Q^2)$ comparable to that of the HW1 model, albeit at the cost of not matching the pion decay constant very well; the second choice led to a prediction for $F_\pi(Q^2)$ similar to that of the SW model.

In the following we shall choose the two free parameters λ and z_0 such that, in addition to the mass of the lightest rho meson, this model reproduces the mass of $\rho(1450)$, which the Particle Data Group [34] lists as 1465 ± 25 MeV. This leads to

$$\lambda z_0 = 1.697, \quad z_0 = 2.9738 \text{ GeV}^{-1}, \quad (2.31)$$

which is right between the two parameter sets explored in [30]. Note that the SHW parameter λ , which determines the behavior of Φ at large z , is significantly larger [≈ 571 MeV in the case of Eq. (2.31)] than the analogous SW parameter $\kappa = m_\rho/2$.

With Eq. (2.30) closed analytical results are no longer available, and one has to resort to numerical solutions of the equations of motion for the vector modes. In contrast to the SW model, m_n^2 becomes a linear function of n only for large n , where the spacing is determined by $m_{n+1}^2 - m_n^2 \sim 4\lambda^2 n$ [$\approx 1.3 \text{ GeV}^2$ for our choice, Eq. (2.31)]. The decay constants are again given by $F_n = \psi_n''(0)/g_5$, with g_5 still determined by Eq. (2.18). Table I lists the results for the first eight modes.

The full subtracted self-energy function with $\Pi_V^{\text{ren}}(0) = 0$ can then be calculated using

$$\Pi_V^{\text{ren}}(-q^2) = \sum_{n=1}^m \frac{q^2 F_n^2}{(q^2 - m_n^2) m_n^4} + \mathcal{O}\left(\frac{q^2}{m_{m+1}^2}\right). \quad (2.32)$$

TABLE I. Vector meson masses m_n and decay constants $F_n^{1/2}$ in MeV (fitted values in italics).

n	HW1		HW2(IR UV fit)		SW		SHW		TC (fit 1 2)	
	m_n	$F_n^{1/2}$	m_n	$F_n^{1/2}$	m_n	$F_n^{1/2}$	m_n	$F_n^{1/2}$	m_n	$F_n^{1/2}$
1	775	329.1	775 987.2	371.4 419.2	775	260.0	775	314.0	765.4 803.9	313.2 329.0
2	1779	615.8	1779 2266	695.1 784.5	1096	309.2	<i>1465</i>	458.5	1382 1453	418.0 438.9
3	2789	863.3	2789 3553	974.4 1100	1342	342.2	1903	498.7	1806 1899	488.7 513.0
4	3800	1089	3800 4841	1229 1387	1550	367.7	2230	540.0	2158 2269	538.4 564.9
5	4812	1300	4812 6130	1467 1656	1733	388.8	2511	570.7	2466 2593	577.3 605.4
6	5824	1500	5824 7419	1693 1911	1898	406.9	2762	597.4	2744 2885	610.4 639.6
7	6836	1692	6836 8708	1909 2155	2050	422.9	2991	621.4	2999 3153	639.4 669.7
8	7848	1876	7848 9997	2118 2390	2192	437.2	3203	642.8	3236 3402	665.5 696.6

2. Tachyon condensation (TC) model

Finally we consider a more sophisticated but still relatively simple bottom-up model, developed in [31–33], where chiral symmetry breaking is implemented using a brane-antibrane effective action with an open string tachyon mode as proposed by Sen [35]. This is based on a pair of Dirac-Born-Infeld type Lagrangians augmented by a tachyon potential $V(|T|)$, which in the case of a single flavor reads

$$S = \int d^4x dz V(|T|) \left(\sqrt{\det \mathbf{A}^{(L)}} + \sqrt{\det \mathbf{A}^{(R)}} \right), \quad (2.33)$$

where

$$\begin{aligned} \mathbf{A}_{MN}^{(L,R)} = & g_{MN} + \frac{2\pi\alpha'}{g_V} F_{MN}^{(L,R)} + \pi\alpha'\lambda[(D_M T)^*(D_N T) \\ & + (D_N T)^*(D_M T)] \end{aligned} \quad (2.34)$$

and

$$D_M T = (\partial_M + iA_M^{(L)} - iA_M^{(R)})T, \quad T = \tau e^{i\theta}, \quad (2.35)$$

with a Gaussian potential

$$V = \mathcal{K} e^{-\frac{1}{2}\mu^2 \tau^2}. \quad (2.36)$$

The background geometry is derived from a six-dimensional AdS soliton, which was proposed by Kuperstein and Sonnenschein as a holographic model of four-dimensional Yang-Mills theory [36]. It is given by

$$ds_5^2 = g_{tt} dt^2 - g_{zz} dz^2 - g_{xx} dx_3^2 = \frac{R^2}{z^2} [dx_{1,3}^2 - f_\Lambda^{-1} dz^2], \quad (2.37)$$

where $f_\Lambda = 1 - (z/z_\Lambda)^5$.

Like the bifundamental scalar X in the HW and SW models, the scalar T mediates chiral symmetry breaking by its possible vacuum solutions. In order to match the scaling dimension of a quark bilinear, the AdS/CFT correspondence requires one to set the mass of the field τ to

$$m_\tau^2 R^2 = -\frac{R^2 \mu^2}{2\pi\alpha'\lambda} = -3, \quad (2.38)$$

which leads to the differential equation for its profile $\tau(z)$,

$$\tau'' - \frac{4\mu^2 z f_\Lambda}{3} \tau^3 + \left(-\frac{3}{z} + \frac{f'_\Lambda}{2f_\Lambda} \right) \tau' + \left(\frac{3}{z^2 f_\Lambda} + \mu^2 \tau^2 \right) \tau = 0, \quad (2.39)$$

and a UV asymptotic behavior parametrized by two constants c_1 and c_3 ,

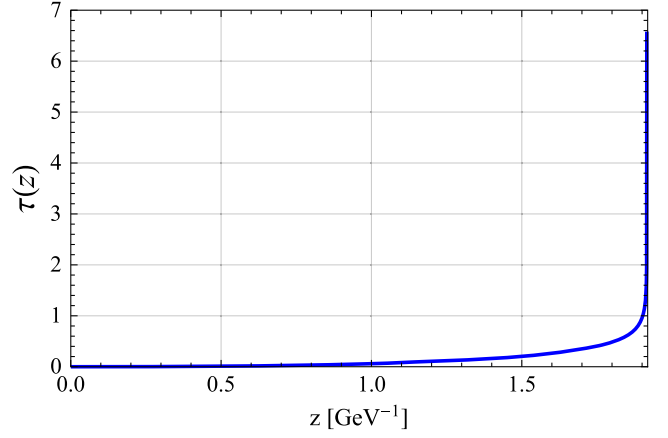


FIG. 1. Tachyon field $\tau(z)$ for the parameters in Eq. (2.41).

$$\tau = c_1 z + \frac{\mu^2}{6} c_1^3 z^3 \ln z + c_3 z^3 + \mathcal{O}(z^5). \quad (2.40)$$

When the source parameter c_1 corresponding to the quark mass is chosen, the parameter c_3 is tuned such that the tachyon diverges exactly at $z = z_\Lambda$.

The parameter μ in the tachyon potential does not have a physical meaning, as it can be absorbed in the definition of τ ; in the following it will be set to $\mu^2 = \pi$. In [32] a fit of light unflavored mesons (composed of u and d quarks) gave

$$z_\Lambda^{-1} = 522 \text{ MeV}, \quad c_1 = 0.0125 z_\Lambda^{-1}. \quad (2.41)$$

We shall refer to this as TC (fit 1). In [33] the parameters are chosen as

$$z_\Lambda^{-1} = 549 \text{ MeV}, \quad c_1 = 0.0094 z_\Lambda^{-1}, \quad (2.42)$$

which gives a slightly higher mass for the lightest rho meson [referred to as TC (fit 2) in the following].

The function $\tau(z)$ that we obtain as the solution of Eq. (2.39) is plotted in Fig. 1. The value that we obtain for the other constant is

$$c_3 \approx 0.37 z_\Lambda^{-3}. \quad (2.43)$$

Given $\tau(z)$, one can proceed by expanding the action (2.33) up to quadratic order in the fields as in the other models above.

For the vector gauge fields $V_\mu = [A_\mu^{(L)} + A_\mu^{(R)}]/2$ and the corresponding field strength $V_{\mu\nu}$, the action up to quadratic order reads

$$\begin{aligned} S_V = & \frac{(2\pi\alpha')^2}{g_V^4} \mathcal{K} \int d^4x dz e^{-\frac{1}{2}\mu^2 \tau^2} \\ & \times \left[\frac{1}{2} \tilde{g}_{zz}^{\frac{1}{2}} V_{\mu\nu} V^{\mu\nu} + g_{xx} \tilde{g}_{zz}^{-\frac{1}{2}} \partial_z V_\mu \partial_z V^\mu \right], \end{aligned} \quad (2.44)$$

where we have defined $\tilde{g}_{zz} = g_{zz} + 2\pi\alpha'\lambda(\partial_z\langle\tau\rangle)^2$. This leads to the mode equations

$$-\frac{1}{e^{-\frac{1}{2}\mu^2\tau^2}\tilde{g}_{zz}^{\frac{1}{2}}}\partial_z(e^{-\frac{1}{2}\mu^2\tau^2}g_{xx}\tilde{g}_{zz}^{-\frac{1}{2}}\partial_z\psi_n(z)) = m_n^2\psi_n(z). \quad (2.45)$$

As in the SHW model, solutions have to be obtained by relying on numerical calculations, which is best done by transforming the differential equations to Liouville normal form (see the Appendix of [33]). The vector correlator, which is given by

$$\Pi_V(-q^2) = -2\frac{(2\pi\alpha')^2\mathcal{K}R}{g_V^4}\frac{\partial_z V(q,z)}{q^2 z}\Big|_{z=\epsilon} \quad (2.46)$$

for a solution with the boundary condition $V(q,0) = 1$, can then be calculated alternatively by summing a sufficiently large number of modes according to Eq. (2.32). The behavior at large q^2 can be shown [33] to be of a form similar to that of the SW model. Matching to the leading-order term of the operator product expansion (OPE) result leads to

$$\frac{2(2\pi\alpha')^2\mathcal{K}R}{g_V^4} = \frac{N_c}{12\pi^2}. \quad (2.47)$$

Like the SHW model, the TC model has a linear dependence of m_n^2 on n only for large n , where it can be shown [33] that the spacing is given by $m_{n+1}^2 - m_n^2 \sim 6z_\Lambda^{-2} [\approx 1.6$ and 1.8 GeV^2 for Eqs. (2.41) and (2.42), respectively].

III. NUMERICAL RESULTS

A. Masses and decay constants

In Table I we list our results for the masses and decay constants of the vector mesons in the various models. In the HW1, SW, and SHW models we have fixed $m_1 = 775 \text{ MeV}$ while setting g_5 such that the asymptotic behavior of the vector correlator is matched. The extra parameter in the SHW model was used to additionally match $m_2 = 1465 \text{ MeV}$, while in the TC model we have considered the two sets presented in [32,33]. The simpler HW2 model, which instead has fewer parameters, is considered in the two versions used in [9,10] for evaluating the HLbL contribution to the muon $g-2$: an IR fit where m_ρ and f_π are matched but short-distance constraints are only satisfied at the level of 61%, and a UV fit where f_π and the short-distance behavior are correct but m_ρ is too heavy by 27%.

In the HW models, the masses of excited rho mesons rise very quickly, asymptotically like $m_n^2 \sim n^2$, whereas the SW, SHW, and TC models have $m_n^2 \sim n$, as required by linear confinement. While in the HW models the first excited rho meson has a mass significantly higher than the

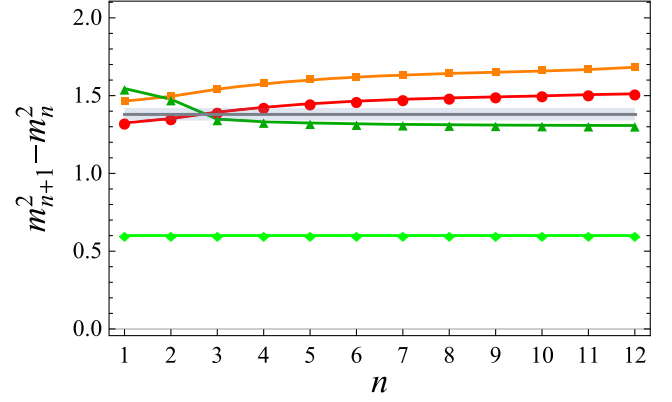


FIG. 2. Plots of $m_{n+1}^2 - m_n^2$ in GeV^2 in models where $m_n^2 \sim n$ for large n : the SW model (light green/diamonds), the SHW model (darker green/triangles), and the TC model (fit 1 in red/disks and fit 2 in orange/squares). The gray line is the phenomenological value given in [37] as $1.38(4) \text{ GeV}^2$, with the gray shaded region representing its uncertainty.

experimental value $m_2 = 1465 \text{ MeV}$, in the simple SW this value is 25% too low. This can be remedied in the SHW by our choice for its parameters, and also by the overall fits [32,33] in the TC model. In the SHW and TC models, m_3 and m_4 are also very compatible with the next states on the radial Regge trajectory, which in [37] were assumed to be $\rho(1900)$ and $\rho(2150)$. In Fig. 2 we plot the increments of the masses squared for the first 12 modes in the models with an asymptotically linear behavior, which shows that the simple SW model has a much smaller value ($m_{n+1}^2 - m_n^2 \equiv m_\rho^2 \approx 0.601 \text{ GeV}^2$) than the SHW and TC models. The latter are in fact closer to the observed slope of radial Regge trajectories, which in [37] was determined as $1.38(4) \text{ GeV}^2$.

Regarding decay constants, sufficient experimental information is available for only the lightest rho meson through $\Gamma(\rho^0 \rightarrow e^+e^-) = 7.04(6) \text{ keV}$ [34], which yields [38]

$$F_{\rho^0}^2 = 3m_\rho^3\Gamma(\rho^0 \rightarrow e^+e^-)/(4\pi\alpha^2) = [348(1) \text{ MeV}]^4. \quad (3.1)$$

The largest deviations from this result, of about 25% and 20%, respectively, are found in the SW model and in the HW2(UV fit) case, whereas the HW1 model deviations are merely 5% too low. Note that $F_n \propto g_5^{-2}$, which implies that one could match the experimental result by a corresponding adjustment of g_5 .

B. $N_f = 2$ LO-HVP contribution to a_μ

In Table II we finally give the results for the leading-order HVP contribution to the anomalous magnetic moment of the muon with two light flavors, $a_{\mu(N_f=2)}^{\text{LO-HVP}}$, by using Eq. (1.4). As mentioned above, for the HW and SW

TABLE II. Values of $a_\mu^{\text{LO-HVP}}$ with $N_f = 2$ for the different hQCD models in multiples of 10^{-10} . The last column gives the ratio of these results over $a_\mu^{\text{LO-HVP}}{}_{\mu(\pi\pi,\pi\pi\pi,\pi\gamma)}$ as obtained in the dispersive approach [Eq. (3.2)].

	$a_\mu^{\text{LO-HVP}}{}_{\mu(N_f=2)}$	Mismatch
HW1	476.9	0.86
HW2(IR UV fit)	773.9 304.0	1.39 0.55
SW	276.4	0.50
SHW	415.4	0.75
TC (fit 1 2)	442.3 403.6	0.79 0.72

models we can use closed form expressions for Π_V .³ For the SHW and TC models, we rely on numerical results and the expansion (2.32). The corresponding integrands in the master formula (1.4) are displayed in Fig. 3.

With the exception of the model HW2 (with fitted m_ρ and f_π), where the asymptotic behavior of Π_V is about a factor of 1.6 larger than the OPE result, the holographic results are much smaller than the results obtained for the $N_f = 2$ contributions in dispersive and lattice approaches (the latter are about 590×10^{-10} [1] and 640×10^{-10} [2], respectively). However, the holographic QCD models should be viewed as (more or less crude) large- N_c approximations. HVP contributions with multihadron states such as four pions correspond to higher-order contributions in the large- N_c expansion, so it appears to be more reasonable to compare only with contributions from intermediate states corresponding to the ρ and ω channels, which are dominated by two- and three-pion states as well as $\pi^0\gamma$. Table III lists their contributions to a_μ according to [39,40], which combined give approximately

$$a_\mu^{\text{LO-HVP}}{}_{\mu(\pi\pi,\pi\pi\pi,\pi\gamma)} = 557(3) \times 10^{-10}. \quad (3.2)$$

While the HW2 model in its two versions brackets this result, with rather large deviations on either side, the HW1 model, where m_ρ and f_π as well as the short-distance behavior can be fitted simultaneously, is only a factor of 0.86 smaller, and thus comes the closest of all models considered here.

The smallest result, at only 50%, is obtained with the SW model. As we have seen above, the SW model with a

³In [13] Π_V in the HW1 model was calculated by truncating the infinite sum in Eq. (2.15) at $n = 4$, which produces a result that is about 1% lower than the full contribution. With the slightly different choice of $m_1 = 775.49$ MeV of [13], we would obtain $a_\mu^{\text{LO-HVP}}{}_{\mu(N_f=2)} = 476.4 \times 10^{-10}$, while the truncated result given in [13] is $a_\mu^{\text{LO-HVP}}{}_{\mu(N_f=2)} = 470.5 \times 10^{-10}$.

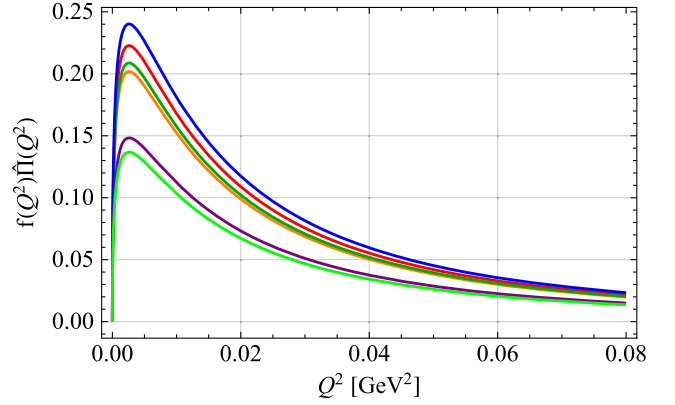


FIG. 3. Plot of the integrand $f(Q^2)\hat{\Pi}(Q^2) = f(Q^2)4\pi^2\Pi_{\text{em}}^{\text{had}}(Q^2)$ in Eq. (1.4) for the HW1 model (blue line; peak value ≈ 0.24), SW model (light green line; 0.14), SHW model (darker green line; 0.21), and the TC model with fit 1 (red line; 0.22) and fit 2 (orange line; 0.20). The HW2 model is shown only in the UV-fit version (purple line; 0.15), where the UV behavior is reproduced at the expense of an unrealistically heavy rho meson; when m_ρ and f_π are fitted, the integrand peaks at about 0.39 and the UV behavior is about a factor of 1.6 too large.

strictly linear dependence of m_n^2 on n underestimates the masses of all excited rho mesons. While this should tend to overestimate $a_\mu^{\text{LO-HVP}}$, the decay constant squared of the ground-state rho meson is at only 30% of its experimental value, which is thus responsible for the strong attenuation. However, the simple modification (2.30) in the SHW model, which leads to a much improved mass spectrum, also brings the decay constants closer to realistic values, yielding a result for $a_\mu^{\text{LO-HVP}}$ that is only 25% below Eq. (3.2). The more sophisticated TC model turns out to be comparable, coming somewhat closer, with parameters of fit 1.

Thus all models which reproduce m_ρ , f_π , and F_{ρ^0} reasonably well also do not deviate too strongly from the dispersive result for $a_\mu^{\text{LO-HVP}}$ but uniformly underestimate it. Since the latter is proportional to g_5^{-2} , this suggests that its value, obtained from matching the leading-order term in the vector correlator (2.17), should be corrected to account for the next-to-leading-order term, which is indeed positive. Exactly such a correction was

TABLE III. Rounded contributions of decay channels with one, two, and three pions to $a_\mu^{\text{LO-HVP}}$ in multiples of 10^{-10} [1].

	DHMZ19 [39]	KNT19 [40]
$\pi^+\pi^-$	508(3)	504(2)
$\pi^+\pi^-\pi^0$	46(1)	47(1)
$\pi^0\gamma$	4.4(1)	4.6(1)
Sum	558(4)	555(3)

proposed by two of us in the evaluation of the HLbL contribution within the (massive) HW1 and HW3 models [11,12], where it has the effect of reducing the holographic HLbL result, as this brings the asymptotic behavior of transition form factors down by amounts that are roughly consistent with perturbative corrections to the leading-order QCD results for moderately high Q^2 values [41,42]. At the same time, the coefficient of the logarithm in the asymptotic expression (2.17) is increased by a similar amount, which is consistent with the next-to-leading-order terms in this expression.

In the case of the HW1 model, F_{ρ^0} can be matched by reducing g_5^2 by a factor of 0.9. This happens to bring the HW1 result for the π^0 pole contribution to the HLbL part of a_μ into perfect agreement with the dispersive result [11]: $a_{\mu(\text{HW1.3})}^{\pi^0} = (6.17\dots 6.39) \times 10^{-10}$, while $a_{\mu(\text{disp})}^{\pi^0} = 6.26_{-25}^{+30} \times 10^{-10}$ [43].

With F_{ρ^0} matched, the HW1 result for $a_\mu^{\text{LO-HVP}}$ becomes correspondingly larger—namely, 533.2×10^{-10} , which is less than 5% smaller than the dispersive result (3.2).⁴

IV. CONCLUSION

By considering a number of simple bottom-up holographic QCD models, we have found that their quantitative predictions are too spread out to be of help with the task of determining the HVP contribution to the anomalous magnetic moment of the muon, which is currently hindered by the largest uncertainty with regard to the ongoing efforts of testing the Standard Model in a new round of experiments. However, a comparison of the holographic results for the LO-HVP contribution with the existing data-driven results at or below percent accuracy allows us to assess the various holographic models with regard to their ability to account for the relevant interactions between hadrons and photons. This is useful because holographic QCD can provide interesting estimates for HLbL contributions, where conventional approaches have uncertainties that are comparable to or larger than expected errors in the large- N_c limit that holographic QCD is based upon.⁵

In particular, we have considered the holographic SW and HW models that have been used previously for estimating the HLbL contributions of pseudoscalars and axial-vector mesons (see the recent review [12]), and we have also explored two simple extensions that aim to interpolate between the HW and SW models while keeping their respective advantages.

We have found that the original HW1 model [16] turned out to come closest to the phenomenological value of the

⁴Interestingly, in [22] it was argued that inclusion of the effects of a gluon condensate within a modified HW1 model leads to an increase of about 6% of the holographic value for $a_\mu^{\text{LO-HVP}}$.

⁵For example, the contribution of axial-vector mesons was assigned a 100% uncertainty in [1].

rho meson decay constant as well as to the value for $a_{\mu(N_f=2)}^{\text{LO-HVP}}$ obtained in dispersive approaches. The somewhat simpler HW2 model, which was used in holographic calculations of the axial-vector contribution in two versions which fit either IR or UV constraints, brackets the latter with rather large deviations in both directions. The SW model turns out to give the worst fit, but the simple improvement of a semihard wall proposed in [28,30] already reduces the deviation considerably; the more sophisticated TC model achieves roughly the same with the parameters considered previously in [31–33].

In the HW1 model, the LO-HVP result is simply proportional to the coupling g_5^{-2} determining the asymptotic behavior of the vector correlator. Reducing g_5^2 by a factor of 0.9 or 0.85 was proposed in [11,12] as a simple way to account for next-to-leading-order QCD effects for the large- Q^2 behavior of transition form factors. In the case of the rho meson decay constant, a factor of 0.9 leads to a perfect fit with the phenomenological value and a result for $a_{\mu(N_f=2)}^{\text{LO-HVP}}$ that is only 5% too small. As shown in [11,12], the same reduction of g_5^2 brings about a perfect agreement of the pion pole contribution in the HW1 model with the data-driven result of [43]. We interpret this as support for the predictions for pseudoscalar and axial-vector meson contributions obtained by two of us in various versions of the HW1 and HW3 model [11,12], where a theoretical error was formed by taking the unchanged results of these models as the upper bound and those with g_5^2 reduced by a factor of 0.85 as the lower bound. The corresponding values with the factor 0.9 could then be regarded as the best guess within these models.⁶

As an outlook we would like to refer to the many possible improvements that can be considered for bottom-up holographic QCD models. In [22] it has already been shown that incorporating the effects of a gluon condensate within a modified HW1 model leads to an increase of about 6% of the holographic value for $a_\mu^{\text{LO-HVP}}$, bringing it very close to the data-driven result. It would be interesting to study even more extensions, such as models that relax the assumption $N_f \ll N_c$ of the 't Hooft limit [44].

ACKNOWLEDGMENTS

J.L. was supported by the FWF doctoral program Particles and Interactions, Project No. W1252-N27, and FWF Project No. P33655. This work has been partially funded by the Deutsche Forschungsgemeinschaft (DFG, German Research Foundation) under Germany's Excellence Strategy—EXC-2094—390783311 and DFG Grant BSMEXPEDITION.

⁶We do not reproduce these numbers here. They can be easily obtained by applying the correction factors given in Table III of [11] to the results in Table II therein.

- [1] T. Aoyama *et al.*, The anomalous magnetic moment of the muon in the Standard Model, *Phys. Rep.* **887**, 1 (2020).
- [2] S. Borsanyi *et al.*, Leading hadronic contribution to the muon magnetic moment from lattice QCD, *Nature* **593**, 51 (2021).
- [3] M. Passera, W. J. Marciano, and A. Sirlin, The muon $g - 2$ and the bounds on the Higgs boson mass, *Phys. Rev. D* **78**, 013009 (2008).
- [4] A. Crivellin, M. Hoferichter, C. A. Manzari, and M. Montull, Hadronic Vacuum Polarization: $(g - 2)_\mu$ versus Global Electroweak Fits, *Phys. Rev. Lett.* **125**, 091801 (2020).
- [5] A. Keshavarzi, W. J. Marciano, M. Passera, and A. Sirlin, Muon $g - 2$ and $\Delta\alpha$ connection, *Phys. Rev. D* **102**, 033002 (2020).
- [6] K. Melnikov and A. Vainshtein, Hadronic light-by-light scattering contribution to the muon anomalous magnetic moment revisited, *Phys. Rev. D* **70**, 113006 (2004).
- [7] J. Lüdtke and M. Procura, Effects of longitudinal short-distance constraints on the hadronic light-by-light contribution to the muon $g - 2$, *Eur. Phys. J. C* **80**, 1108 (2020).
- [8] G. Colangelo, F. Hagelstein, M. Hoferichter, L. Laub, and P. Stoffer, Short-distance constraints for the longitudinal component of the hadronic light-by-light amplitude: An update, *Eur. Phys. J. C* **81**, 702 (2021).
- [9] J. Leutgeb and A. Rebhan, Axial vector transition form factors in holographic QCD and their contribution to the anomalous magnetic moment of the muon, *Phys. Rev. D* **101**, 114015 (2020).
- [10] L. Cappiello, O. Catà, G. D'Ambrosio, D. Greynat, and A. Iyer, Axial-vector and pseudoscalar mesons in the hadronic light-by-light contribution to the muon $(g - 2)$, *Phys. Rev. D* **102**, 016009 (2020).
- [11] J. Leutgeb and A. Rebhan, Hadronic light-by-light contribution to the muon $g - 2$ from holographic QCD with massive pions, *Phys. Rev. D* **104**, 094017 (2021).
- [12] J. Leutgeb, J. Mager, and A. Rebhan, Holographic QCD and the muon anomalous magnetic moment, *Eur. Phys. J. C* **81**, 1008 (2021).
- [13] D. K. Hong, D. Kim, and S. Matsuzaki, Holographic calculation of hadronic contributions to muon $g - 2$, *Phys. Rev. D* **81**, 073005 (2010).
- [14] T. Blum, Lattice Calculation of the Lowest Order Hadronic Contribution to the Muon Anomalous Magnetic Moment, *Phys. Rev. Lett.* **91**, 052001 (2003).
- [15] C. Aubin and T. Blum, Calculating the hadronic vacuum polarization and leading hadronic contribution to the muon anomalous magnetic moment with improved staggered quarks, *Phys. Rev. D* **75**, 114502 (2007).
- [16] J. Erlich, E. Katz, D. T. Son, and M. A. Stephanov, QCD and a Holographic Model of Hadrons, *Phys. Rev. Lett.* **95**, 261602 (2005).
- [17] L. Da Rold and A. Pomarol, Chiral symmetry breaking from five-dimensional spaces, *Nucl. Phys.* **B721**, 79 (2005).
- [18] J. Hirn and V. Sanz, Interpolating between low and high energy QCD via a 5D Yang-Mills model, *J. High Energy Phys.* **12** (2005) 030.
- [19] O. Domènech, G. Panico, and A. Wulzer, Massive pions, anomalies and baryons in holographic QCD, *Nucl. Phys.* **A853**, 97 (2011).
- [20] M. A. Shifman, A. I. Vainshtein, and V. I. Zakharov, QCD and resonance physics. Theoretical foundations, *Nucl. Phys.* **B147**, 385 (1979).
- [21] L. Reinders, H. Rubinstein, and S. Yazaki, Hadron properties from QCD sum rules, *Phys. Rep.* **127**, 1 (1985).
- [22] M. Kurachi, S. Matsuzaki, and K. Yamawaki, Gluonic effects on $g - 2$: Holographic view, *Phys. Rev. D* **88**, 055001 (2013).
- [23] Z. Abidin and C. E. Carlson, Strange hadrons and kaon-to-pion transition form factors from holography, *Phys. Rev. D* **80**, 115010 (2009).
- [24] L. Cappiello, O. Cata, and G. D'Ambrosio, The hadronic light by light contribution to the $(g - 2)_\mu$ with holographic models of QCD, *Phys. Rev. D* **83**, 093006 (2011).
- [25] J. Leutgeb, J. Mager, and A. Rebhan, Pseudoscalar transition form factors and the hadronic light-by-light contribution to the anomalous magnetic moment of the muon from holographic QCD, *Phys. Rev. D* **100**, 094038 (2019); Erratum, *Phys. Rev. D* **104**, 059903 (2021).
- [26] A. Karch, E. Katz, D. T. Son, and M. A. Stephanov, Linear confinement and AdS/QCD, *Phys. Rev. D* **74**, 015005 (2006).
- [27] K. Ghoroku, N. Maru, M. Tachibana, and M. Yahiro, Holographic model for hadrons in deformed AdS₅ background, *Phys. Lett. B* **633**, 602 (2006).
- [28] H. J. Kwee and R. F. Lebed, Pion form-factors in holographic QCD, *J. High Energy Phys.* **01** (2008) 027.
- [29] H. R. Grigoryan and A. V. Radyushkin, Structure of vector mesons in holographic model with linear confinement, *Phys. Rev. D* **76**, 095007 (2007).
- [30] H. J. Kwee and R. F. Lebed, Pion form factor in improved holographic QCD backgrounds, *Phys. Rev. D* **77**, 115007 (2008).
- [31] R. Casero, E. Kiritsis, and A. Paredes, Chiral symmetry breaking as open string tachyon condensation, *Nucl. Phys.* **B787**, 98 (2007).
- [32] I. Iatrakis, E. Kiritsis, and A. Paredes, An AdS/QCD model from Sen's tachyon action, *Phys. Rev. D* **81**, 115004 (2010).
- [33] I. Iatrakis, E. Kiritsis, and A. Paredes, An AdS/QCD model from tachyon condensation: II, *J. High Energy Phys.* **11** (2010) 123.
- [34] P. A. Zyla *et al.* (Particle Data Group), Review of particle physics, *Prog. Theor. Exp. Phys.* **2020**, 083C01 (2020).
- [35] A. Sen, Dirac-Born-Infeld action on the tachyon kink and vortex, *Phys. Rev. D* **68**, 066008 (2003).
- [36] S. Kuperstein and J. Sonnenschein, Non-critical, near extremal AdS₆ background as a holographic laboratory of four dimensional YM theory, *J. High Energy Phys.* **11** (2004) 026.
- [37] P. Masjuan, E. Ruiz Arriola, and W. Broniowski, Systematics of radial and angular-momentum Regge trajectories of light nonstrange $q\bar{q}$ -states, *Phys. Rev. D* **85**, 094006 (2012).
- [38] J. F. Donoghue, E. Golowich, and B. R. Holstein, *Dynamics of the Standard Model*, 2nd ed. (Cambridge University Press, Cambridge, England, 2014), 10.1017/CBO9780511803512.
- [39] M. Davier, A. Hoecker, B. Malaescu, and Z. Zhang, A new evaluation of the hadronic vacuum polarisation contributions to the muon anomalous magnetic moment and to $\alpha(m_Z^2)$, *Eur. Phys. J. C* **80**, 241 (2020).

- [40] A. Keshavarzi, D. Nomura, and T. Teubner, $g - 2$ of charged leptons, $\alpha(M_Z^2)$, and the hyperfine splitting of muonium, *Phys. Rev. D* **101**, 014029 (2020).
- [41] B. Melić, D. Müller, and K. Passek-Kumerički, Next-to-next-to-leading prediction for the photon to pion transition form-factor, *Phys. Rev. D* **68**, 014013 (2003).
- [42] J. Bijnens, N. Hermansson-Truedsson, L. Laub, and A. Rodríguez-Sánchez, The two-loop perturbative correction to the $(g - 2)_\mu$ HLbL at short distances, *J. High Energy Phys.* **04** (2021) 240.
- [43] M. Hoferichter, B.-L. Hoid, B. Kubis, S. Leupold, and S. P. Schneider, Dispersion relation for hadronic light-by-light scattering: Pion pole, *J. High Energy Phys.* **10** (2018) 141.
- [44] M. Järvinen and E. Kiritsis, Holographic models for QCD in the Veneziano limit, *J. High Energy Phys.* **03** (2012) 002.